

Low temperature back-surface-field contacts deposited by Hot-wire CVD for heterojunction solar cells

D. Muñoz^{1*}, C. Voz¹, I. Martín¹, A. Orpella¹, R. Alcubilla¹, F. Villar²,
J. Bertomeu², J. Andreu², P. Roca-i-Cabarrocas³

¹Universitat Politècnica de Catalunya, Grup de Recerca en Micro i Nanotecnologies,
Jordi Girona 1-3, Barcelona 08034, Spain

²CeRMAE -Universitat de Barcelona, Departament de Física Aplicada i Òptica,
Diagonal 647, Barcelona 08028, Spain

³LPICM- Ecole Polytechnique, CNRS 91128 Palaiseau, France

*Corresponding author: Delfina Muñoz, tel. +34934017488, fax. +34934016756, email. delfina@eel.upc.edu

Abstract

The growing interest in using thinner wafers (<200 μm) requires the development of low temperature passivation strategies for the back contact of heterojunction solar cells. In this work, we investigate low temperature deposited back contacts based on boron-doped amorphous silicon films obtained by Hot-Wire CVD. The microstructure of the deposited thin films has been comprehensively studied by Spectroscopic Ellipsometry in the UV-visible range. The effective recombination velocity at the back surface has been measured by the Quasi-Steady-State Photoconductance technique. Complete double-side heterojunction solar cells (1 cm^2) have been fabricated with total-area conversion efficiencies up to 14.5%.

Keywords

Hot-wire deposition, Solar cell, Heterostructure

1. Introduction

The investigation of heterojunction silicon solar cells has gained much interest since Sanyo reported outstanding conversion efficiencies over 20% with its so-called HIT (Heterojunction with Intrinsic Thin layer) solar cell structure [1]. Although Sanyo uses the HIT structure on both sides of n-type c-Si substrates, most groups limit their investigation to the heterojunction emitter on p-type wafers [2, 3] due to the difficulty in obtaining good quality boron-doped a-Si:H films by the usual deposition techniques. In the case of p-type c-Si substrates, an aluminum back-surface-field (Al-BSF) is usually used as a back contact to focus on understanding and optimizing the heterojunction emitter. The standard industrial process to form the Al-BSF is the alloying of an aluminum screen-printing paste ($\sim 20 \mu\text{m}$) at relatively high temperatures (700-800°C). The effective surface recombination velocity (S_{eff}) obtained with optimized Al-BSF contacts can not be reduced much below 10^3 cm/s [4]. Besides, wafer warping during the cooling process is a severe drawback of Al-BSF contacts, especially taking into account the present efforts to fabricate solar cells with wafers thinner than $200 \mu\text{m}$ [5]. Alternatively, excellent surface passivation can be achieved with low temperature deposited dielectric films such as silicon nitride [6] or silicon carbide [7]. This approach is superior to the Al-BSF contact due to its much lower surface recombination velocity ($S_{\text{eff}} < 100 \text{ cm/s}$), but requires a point contact patterning of the backside as proposed with the PERC (Passivated Emitter and Rear Cell) concept [8]. Point contact formation based on photolithography is unlikely to succeed in industrial production, but the recently developed laser fired contact (LFC) technology has really great potential for future

applications [9]. Nevertheless, the laser set-up and the beam positioning system introduce a relatively complex additional process. On the other hand, low-temperature deposited BSF contacts based on heavily boron-doped thin silicon films have been much less studied, though their implementation in solar cells could be straightforward [10]. The main reason is the already mentioned lower electronic quality of deposited (p)a-Si:H films.

Although most groups, included Sanyo, use the Plasma-Enhanced Chemical Vapour Deposition (PECVD) to grow the a-Si:H films, the Hot-Wire CVD (HWCVD) technique has also recently demonstrated its potential to fabricate state-of-the-art heterojunction silicon solar cells [2]. In the HWCVD technique, besides some technological advantages, the absence of ion bombardment reduces the damage to the c-Si surface. During the last years, our group has also obtained good results in heterojunction solar cells by HWCVD and a conversion efficiency of 15.4% was recently reported [11]. In particular, the optimized heterojunction emitters with structure (n)a-Si:H/(i)a-Si:H/(p)c-Si showed implicit V_{oc} values close to 690 mV measured by the Quasi-Steady-State Photoconductance (QSS-PC) technique. However, the actual V_{oc} is limited to lower values (630 mV) in the final devices, due to the Al-BSF contact used at the rear side. Therefore, we explore the reduction of back surface recombination by means of low temperature deposited BSF contacts based on boron-doped a-Si:H films with and without intrinsic buffer layer. This work includes the microstructural characterization of these samples by Spectroscopic Ellipsometry (SE) in the visible-UV range. In addition, the QSS-PC technique was used to measure the S_{eff} values that can be obtained with these low temperature deposited back contacts. Finally, complete double-side heterojunction solar cells were fabricated on p-type c-Si substrates.

2. Experimental

All the heterostructures presented in this work were obtained on p-type (0.95 $\Omega\cdot\text{cm}$) FZ silicon wafers with (100) crystalline orientation and thickness of 300 μm . Before deposition, silicon wafers were cleaned in a $\text{H}_2\text{SO}_4\text{:H}_2\text{O}_2$ (2:1) solution. Then, dipped in 5% HF until they become hydrophobic and immediately introduced into the load lock chamber of the ultra-high vacuum deposition system. All the thin silicon films were grown by HWCVD under the deposition conditions summarized in Table I. Separate chambers were used to grow the doped and intrinsic thin silicon films to avoid cross-contamination. The wire configuration of both chambers consisted on two parallel tantalum wires 0.5 mm in diameter separated 3 cm, with the gas inlet centered 1 cm below the wires. The substrate is placed 4 cm above the plane of the wires. The deposition conditions for the boron-doped layers have been extensively investigated for this configuration, as it was previously done for the phosphorous-doped ones [11].

In this work, four different low temperature deposited BSF contacts have been considered. These structures incorporate p-type a-Si:H layers of two different doping levels (Table I) deposited either with a 5 nm intrinsic buffer layer or directly on the c-Si surface. In order to easily identify these samples, they have been labelled P, IP, P⁺ and IP⁺. The microstructure of these films is deduced from the fit to the pseudodielectric function ($\epsilon=\epsilon_1+i\epsilon_2$) measured by SE according to the Bruggeman model [12]. On the other hand, the passivating properties of the different low temperature deposited BSF contacts were assessed by the contactless QSS-PC measurement. In this technique, the S_{eff} value is obtained as a function of an average excess minority carrier density (Δn) [13]. Finally, complete double-side heterojunction solar cells were fabricated with the different low temperature BSF contacts under study. In all cases, the heterojunction emitter was the stack of a very thin intrinsic buffer layer (5 nm) followed by a 20 nm

thick (n)a-Si:H film (Table I). The front contact consisted in an indium-tin-oxide (ITO) anti-reflecting coating (80 nm) deposited by RF magnetron sputtering, followed by an evaporated silver grid (2 μm) with 8% shadowing. The active area of the solar cell is 1 cm^2 . The rear contact is finished with a stack of ITO (80 nm) and silver (1 μm) deposited on the (p)a-Si:H film.

3. Results & Discussion

We have measured the imaginary part (ϵ_2) of the pseudo-dielectric function by SE for all the samples under study. The experimental curves have been fitted according to the Bruggeman model. As an example, in figure 1 we show the experimental (symbols) and calculated (lines) data for the two samples without buffer layer (P, P⁺). From the raw data, amorphous structures are expected as no crystalline features are visible. The high values of ϵ_2 indicate that the films are rather dense. The model used to fit the SE data considers a structure consisting of an interface-layer with the c-Si substrate, followed by the main layer and a small surface roughness. The thicknesses, crystalline (X_c), amorphous (X_a) and void fractions (X_v) for all the samples under study are summarized in table 2.

The interface layer is very similar in the samples with intrinsic buffer (IP, IP⁺) without significant influence of the doping level. The microstructure is amorphous with a low void fraction X_v (15-17%) that could indicate moderate hydrogen content. On the other hand, without buffer layer (P, P⁺), the microstructure of the interface strongly depends on the doping level. The P sample presents a significantly denser interface ($X_v=8\%$) compared to the P⁺ one ($X_v=30\%$). We suggest that this difference can be due to the creation of boron–hydrogen complexes in the highly doped sample. Concerning the main layer, all the samples are dense with negligible void fraction. The samples with

lower doping level (P, IP) show the presence of a crystalline fraction X_c (16-17%), whereas the highly doped ones (P^+ , IP^+) are basically amorphous. Finally, the surface roughness did not evidence significant differences in any case.

Figure 2 shows the QSS-PC data corresponding to the studied low-temperature deposited BSF contacts. These results must be discussed considering not only the microstructure depicted by SE measurements, but also the field-effect passivation given by the doping level. When no intrinsic buffer layer is used, the best result was obtained with the highly doped sample P^+ ($S_{\text{eff}}=140$ cm/s). The P sample shows a S_{eff} value about 1000 cm/s, comparable to what could be obtained with typical Al-BSF contacts. As it could be expected, this behaviour agrees with a higher field-effect passivation when the doping level was increased. The introduction of the intrinsic buffer layer improves the passivation quality for both doping levels (IP, IP^+). This effect could be attributed to a reduced defect density at the interface compared to the case when the doped layers are grown directly on the c-Si surface. The S_{eff} measured for IP and IP^+ samples reaches similar values at high injection levels, when recombination is mainly determined by the interface density of states and the importance of field-effect passivation becomes lower. This result indicates similar interfaces in agreement with SE data (Table II). The lower field-effect passivation in the IP sample leads to a higher dependence of S_{eff} on Δn resulting in a value of 294 cm/s at 1-sun irradiance, whereas IP^+ sample maintains a low S_{eff} value of 96 cm/s.

Complete double-side heterojunction solar cells were fabricated incorporating the different low temperature BSF contacts. Figure 3 shows the J-V curves measured under AM1.5 irradiance for these devices. The electrical parameters are summarized in table III and compared to a previous result using a traditional Al-BSF contact.

The P and IP low temperature BSF contacts allowed performances comparable to the one obtained with an Al-BSF contact. Especially remarkable are the relatively high V_{oc} values exceeding 610 mV in a fully low temperature process by HWCVD (<200 °C). It is also worth mentioning that the FF value of the P device is even better than the one obtained with an Al-BSF contact. Unfortunately, the solar cells incorporating P^+ and IP^+ back contacts with lower S_{eff} values (Fig. 2) evidenced “S-shaped” J-V curves. This effect has been previously reported by different groups, but concerning different heterojunction emitters with traditional back contacts and it is attributed to an unfavourable energy band configuration for carrier collection [14, 15]. The highly doped P^+ and IP^+ back contacts present an essentially amorphous microstructure (Table II), in contrast to the significant crystalline fraction present in the case of lower doping levels (P, IP). This variation should lead to higher band discontinuities that seem to degrade the carrier collection at the back contact. We suggest that the work function of the ITO layer could not be high enough and an inverted Schottky barrier would be created in the interface between the ITO and the $(p^+)a\text{-Si:H}$ film, as reported in Ref. [16] Nevertheless, further research is necessary to gain knowledge about the energy band configuration at the back contact.

Finally, figure 4 shows the External Quantum Efficiency (EQE) curves of the double-side heterojunction solar cells with low doping BSF contacts (P,IP) and with an Al-BSF contact. Since the heterojunction emitter is the same in all cases, the lower response of the IP device in the short wavelength range ($\lambda < 600$ nm) is attributable to differences in the quality of the front contact, namely the ITO antireflection coating. In the long wavelength range ($\lambda > 900$ nm), the response with the low temperature IP back contact is very close to the case with a traditional Al-BSF. By contrast, the P back contact does not reach the quality of the other cases as expected from the S_{eff} value. The

behaviour of the EQE curves agrees with the differences observed in the J_{sc} values of the solar cells (Table III).

4. Conclusions

Low temperature deposited BSF contacts based on boron-doped a-Si:H films deposited by HWCVD have been used to replace traditional high temperature Al-BSF contacts. To date, double-side heterojunction solar cells by HWCVD with conversion efficiencies of 14.5% have been already obtained in a fully low temperature process (<200 °C). QSS-PC measurements evidence that an intrinsic buffer layer reduces the interface recombination at the back surface leading to lower S_{eff} values. Structural characterization by SE indicates the amorphization of highly boron-doped films. Despite the higher field-effect passivation of these films, the band configuration is unfavourable as a back contact in finished devices. Further research is necessary considering alternatives to the back ITO layer in order to completely succeed in this approach.

Acknowledgments

This work was developed in the framework of CeRMAE. It has also been supported by the Spanish Government under programme ENE2004-07376-C03-01 and TEC2005-02716/MIC. One of the authors (D.Muñoz) acknowledges the support for the grant program (FI/BE) of the Catalan Government.

References

- [1] M. Taguchi, K. Kawamoto, S. Tsuge, T. Baba, H. Sakata, M. Morizane, K. Uchihashi, N. Nakamura, S. Kiyama and O. Oota, *Prog. Photovolt.: Res. Appl.* 8 (2000) 503.
- [2] T.H. Wang, E. Iwaniczko, M.R. Page, D.H. Levi, Y. Yan, H.M. Branz and Q. Wang, *Thin Solid Films* 501 (2006) 284.
- [3] Y. Veschetti, J.-C. Muller, J. Damon-Lacoste, P. Roca i Cabarrocas, A.S. Gudovskikh, J.-P. Kleider, P.-J. Ribeyron and E. Rolland, *Thin Solid Films* 511 (2006) 543.
- [4] J.W. Jeong, A. Rohatgi, V. Yelendur, A. Ebong, M.D. Rosenblum, J.P. Kalejs, *IEEE Transactions on Electron Devices* 48 (2001) 2836.
- [5] T.M. Bruton, S. Roberts, K.C. Heasman, R. Russel, W. Warta, S.W. Glunz, J. Dicker, J. Knobloch, *Proc.of 28th IEEE Photovoltaic Specialists Conference*, (2000) 180.
- [6] A. G. Aberle and R. Hezel, *Prog. Photovoltaics* 5, (1997) 29.
- [7] I. Martin, M. Vetter, A. Orpella, J. Puigdollers, A. Cuevas, R. Alcubilla, *Appl. Phys. Lett.* 79, (2001) 2199.
- [8] M.A Green, A.W. Blakers, J. Zhao, A.M. Milne, A. Wang, X. Dai, *IEEE Transactions on Electron Devices* 37 (1990) 331.
- [9] E. Schneiderlöchner, R. Preu, R. Lüdemann, S.W. Glunz, *Prog. Photovolt: Res. Appl.* 10 (2002) 29.
- [10] K.V. Maydell, E. Conrad, M. Schmidt *Prog. Photovolt: Res. Appl.* 14 (2006) 289.
- [11] D. Muñoz, C. Voz, I. Martin, A. Orpella, J. Puigdollers, R. Alcubilla, F. Villar, J. Bertomeu, J. Andreu, J. Damon-Lacoste, P. Roca i Cabarrocas, *Thin Solid Films*, in press.

- [12] A. Fontcuberta-i-Morrà, P. Roca-i-Cabarrocas, C. Clerc, *Physical Review B*, 69 (2004) 125307.
- [13] R.A. Sinton, A. Cuevas, *Appl. Phys. Lett.* 69 (1996) 2510.
- [14] A. Froitzheim, K. Brendel, L. Elstner, W. Fuhs, K. Kliefoth and M. Schmidt, *J. Non-Cryst. Solids*, 299 (2002) 663.
- [15] T. Unold, M. Rösch, G.H. Bauer, *J. Non-Cryst. Solids* 266 (2000) 1033.
- [16] E. Centurioni, D. Iencinella, *Electron Device Letters, IEEE* 24 (2003) 177.

List of table and figure captions

Table I: Deposition conditions used to grow the silicon films of the bifacial heterojunction solar cells. The wire temperature was 1600°C for intrinsic a-Si:H and n-doped films, but 1750 °C for p-doped films. The doping precursors were phosphine and diborane for n- and p-type films, respectively.

Table II. Layer structure and composition deduced from the fittings to SE measurements for the four low temperature deposited BSF contacts.

Table III. Electrical parameters of the J-V curves measured under AM1.5 irradiance for the heterojunction solar cells fabricated with the different low temperature BSF contacts. The result obtained with the same emitter but a traditional Al-BSF is included for comparison [11].

Figure 1. Imaginary part of the pseudo-dielectric function measured by SE for the two samples without intrinsic buffer layer (symbols). The lines are the result of the fit with the optical model given in table II.

Figure 2. S_{eff} values as a function of Δn measured by QSS-PC for the four samples under study. The arrows point the values at one-sun irradiance.

Figure 3. J-V characteristics measured under AM1.5 irradiance ($100 \text{ mW}\cdot\text{cm}^{-2}$) for the fabricated double-side heterojunction solar cells.

Figure 4. External Quantum Efficiency curves of the double-side heterojunction solar cells with P and IP BSF contacts compared to the case with a traditional Al-BSF contact.

film	T _s (°C)	H ₂ (sccm)	SiH ₄ (sccm)	Doping (sccm)	Pressure (mbar)
i	100	-	2	-	3.5×10 ⁻³
n	200	28	2	0.04	8×10 ⁻²
p	100	2	1.5	0.02	1×10 ⁻²
p ⁺	100	4	2	0.04	2×10 ⁻²

Table I

MODEL		P	P ⁺	IP	IP ⁺
ROUGHNESS	thickness (nm)	4	5	5	5.5
LAYER	thickness (nm)	30	46	53	57
	Xc (%)	17	2	16	3
	Xa (%)	83	98	84	97
INTERFACE LAYER	thickness (nm)	14	13	17	16
	Xv (%)	8	30	15	17
	Xa (%)	92	70	85	83
c-Si WAFER					

Table II

SAMPLE	V_{oc} (mV)	J_{sc} (mA/cm ²)	FF (%)	η (%)
P	613	30.3	77.9	14.5
IP	618	29.6	75.0	13.7
P ⁺	500	13.6	S-shaped	-
IP ⁺	645	29.2	S-shaped	-
Al-BSF	616	31.4	75.5	14.6

Table III

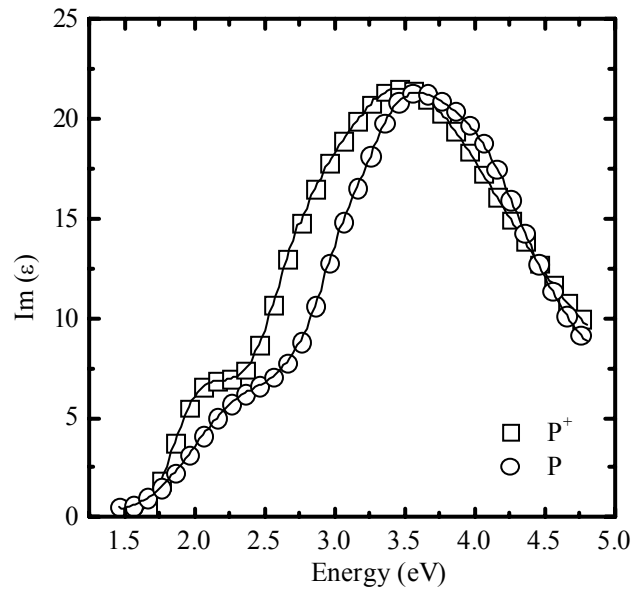


Figure 1

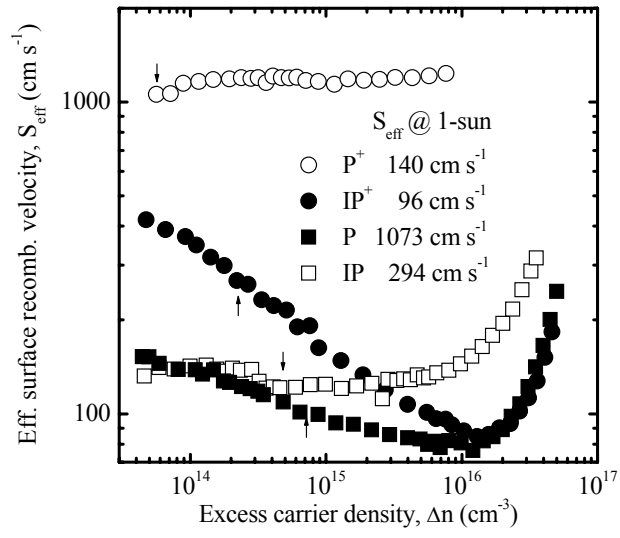


Figure 2

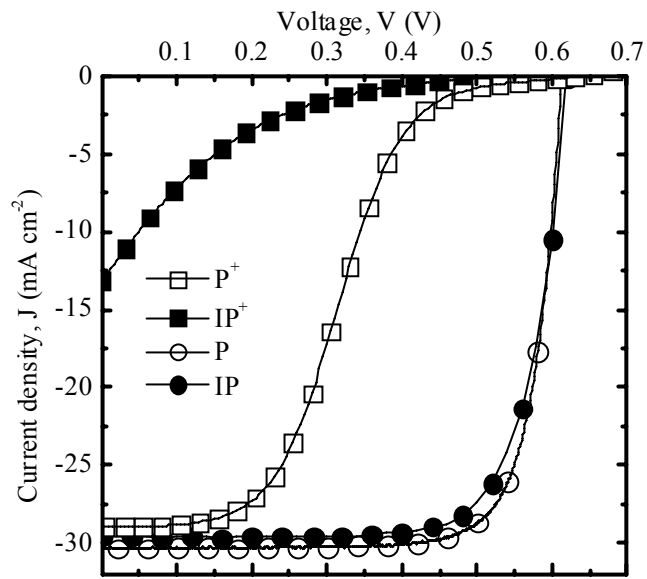


Figure 3

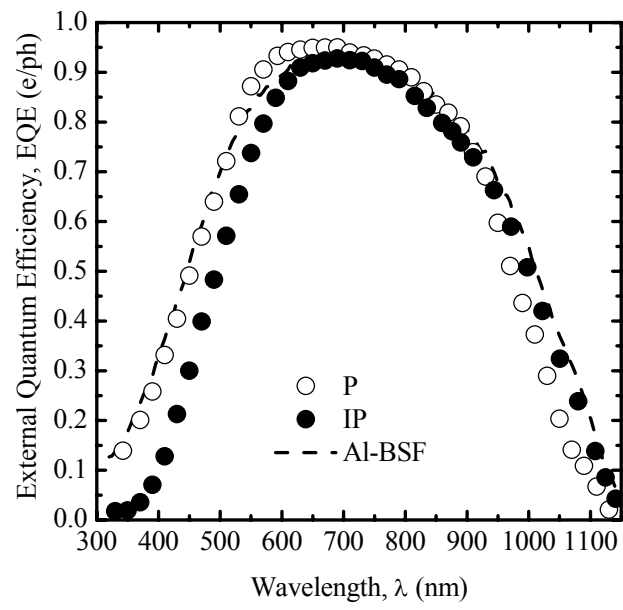


Figure 4